Cell Reports

Resource

# Dissecting the spermatogonial stem cell niche using spatial transcriptomics

## Graphical abstract

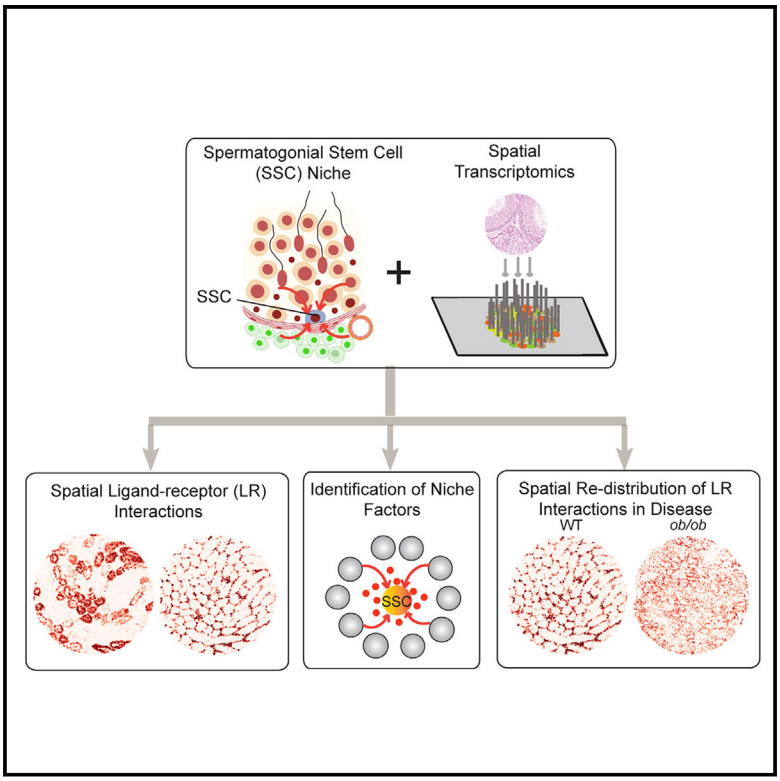


## Highlights

- Inference of ligand-receptor (LR) pairs at the spermatogonial stem cell niche
- PTN and EPHA1 are potential niche factors
- Spatial alteration of LR pair expression underlies diabetes-induced infertility


## Authors

Shreya Rajachandran, Xin Zhang, Qiqi Cao, ..., Makoto Nagano, Kyle E. Orwig, Haiqi Chen

## Correspondence

haiqi.chen@utsouthwestern.edu



## In brief

Rajachandran et al. demonstrate how spatial transcriptomics can be leveraged to identify niche factors that regulate spermatogonial stem cell functions by mapping the ligand-receptor interaction landscape in mouse and human testes.


Rajachandran et al., 2023, Cell Reports *42*, 112737
July 25, 2023 
https://doi.org/10.1016/j.celrep.2023.112737

CellPress

Cell Reports

CellPress
OPEN ACCESS

Resource

# Dissecting the spermatogonial stem cell niche using spatial transcriptomics

Shreya Rajachandran,[1,2,6] Xin Zhang,[1,2,6] Qiqi Cao,[1,2,6] Andre L. Caldeira-Brant,[3] Xiangfan Zhang,[4,5] Youngmin Song,[4,5] Melanie Evans,[2] Orhan Bukulmez,[2] Edward J. Grow,[1,2] Makoto Nagano,[4,5] Kyle E. Orwig,[3] and Haiqi Chen[1,2,7,*]

[1]Cecil H. and Ida Green Center for Reproductive Biology Sciences, University of Texas Southwestern Medical Center, Dallas, TX, USA
[2]Department of Obstetrics and Gynecology, University of Texas Southwestern Medical Center, Dallas, TX, USA
[3]Department of Obstetrics, Gynecology and Reproductive Sciences, Magee-Womens Research Institute, University of Pittsburgh School of Medicine, Pittsburgh, PA, USA
[4]Department of Obstetrics and Gynecology, McGill University, Montreal, QC, Canada
[5]Child Health and Human Development Program, Research Institute of the McGill University Health Centre, Montreal, QC, Canada
[6]These authors contributed equally
[7]Lead contact
*Correspondence: haiqi.chen@utsouthwestern.edu
https://doi.org/10.1016/j.celrep.2023.112737

## SUMMARY

Spermatogonial stem cells (SSCs) in the testis support the lifelong production of sperm. SSCs reside within specialized microenvironments called "niches," which are essential for SSC self-renewal and differentiation. However, our understanding of the molecular and cellular interactions between SSCs and niches remains incomplete. Here, we combine spatial transcriptomics, computational analyses, and functional assays to systematically dissect the molecular, cellular, and spatial composition of SSC niches. This allows us to spatially map the ligand-receptor (LR) interaction landscape in both mouse and human testes. Our data demonstrate that pleiotrophin regulates mouse SSC functions through syndecan receptors. We also identify ephrin-A1 as a potential niche factor that influences human SSC functions. Furthermore, we show that the spatial re-distribution of inflammation-related LR interactions underlies diabetes-induced testicular injury. Together, our study demonstrates a systems approach to dissect the complex organization of the stem cell microenvironment in health and disease.

## INTRODUCTION

In the mammalian testis, spermatogonial stem cells (SSCs) reside in the basal compartment of the seminiferous epithelium (Figure S1A). SSCs self-renew to maintain a constant pool throughout the life cycle of a male adult. They also differentiate, through a series of steps, to amplify the number of sperm. It is believed that the cellular microenvironments (also known as niches) in which SSCs reside play critical roles in regulating SSC self-renewal and differentiation.[1–4] Classically, the functional interaction between SSCs and their niches has been studied using genetic approaches that involve labeling cell types and ablating candidate secreted factors. These studies have generated important insights into the functional roles and cellular sources of key niche factors. For example, Sertoli cells, the only somatic cell type in the seminiferous epithelium, and endothelial cells near the vasculature and the interstitium secrete the glial cell-derived neurotrophic factor (GDNF) that acts on SSCs to support the lifelong maintenance of the SSC pool.[5,6] Retinoic acid (RA), produced primarily by Sertoli cells, mediates the commitment of a sub-group of SSCs to differentiation.[7,8] Additionally, fibroblast growth factors (FGFs) secreted by Sertoli cells and endothelial cells were found to regulate the density and the size of the SSC population.[9,10]

Although powerful, genetic approaches are difficult to scale, making it challenging to identify niche factors that are important to SSC activities. High-throughput molecular profiling technologies such as single-cell RNA sequencing (scRNA-seq) have recently been used to map ligand-receptor (LR) interactions between SSCs and cellular components of the niches.[11,12] However, the LR activities inferred from scRNA-seq data often contain significant false positives, as LR interactions take place within a certain range of spatial distance that is not measured in scRNA-seq datasets. Previous methods for extracting spatial information from the tissues such as individual-cell laser-capture microdissection or multiplexed *in situ* hybridization are low throughput and require prior knowledge of the cell types or the genes to be targeted.[13,14] Therefore, an unbiased, high-throughput molecular profiling method capable of capturing cell-cell interactions within the native context of the testis is needed to further understand the regulation of SSC functions.

We have recently established a spatial transcriptomics workflow to faithfully recapitulate the mouse and human spermatogenesis at the cellular level.[15] Here, using high-resolution spatial transcriptomics and computational analyses, we generated a spatially resolved LR interaction map of the mouse and human testis. Using this map, we showed that SSCs interact with

various niche components through distinct LR mechanisms. We also showed that pleiotrophin (PTN), secreted by Leydig cells and endothelial cells, regulates SSC functions through syndecan (SDC) receptors in the mouse testis. In the human testis, we identified ephrin-A1 ligand (EFNA1) as a potential niche factor. Furthermore, we found that many LR-mediated signaling exhibit cell type- or region-specific activities in both the mouse and human testis. Finally, we identified a selective group of immune response associated LR pairs whose spatial expression patterns alter significantly in the testes of diabetic mice vs. wild-type (WT) mice. Together, we demonstrated the power of high-resolution spatial transcriptomics in dissecting cell-cell communications in the SSC niches at the molecular level. Our study also provides a generalized approach to characterize tissue microenvironment under both physiological and pathological conditions.

## RESULTS

### A spatially resolved LR interaction map of the mouse testis

We recently established a workflow to spatially map major mouse testicular cell types including spermatogonia (SPG) using a spatial transcriptomics approach called Slide-seq.[15] To enable accurate mapping of the SSCs within the SPG population, we generated new Slide-seq datasets from mouse testes and combined them with the previous Slide-seq datasets.[15] A scRNA-seq study previously identified four SPG subtypes that follow the order of SPG1 to SPG4 on the basis of transcriptome patterns and developmental ordering of cells.[16] Marker gene analysis of the scRNA-seq data suggests that cells in SPG1 correspond to undifferentiated SPG, which contain the SSC population, as they express one or more SSC genes, such as *Gfra1*, *Etv5*, and *Eomes*, and lack the expression of differentiation markers[16] (Figure S1B). Unlike SPG1, cells in SPG2–4 express various differentiation marker genes, such as *Kit* and *Stra8*[16] (Figure S1B), suggesting that they represent progressively differentiating SPG. Using a robust cell type decomposition (RCTD) method,[17] we identified and spatially mapped SPG1–4 in the Slide-seq data (Figures 1A and S1C). The accuracy of the mapping of SPG subtypes was confirmed by their spatial localizations at the basal compartment of seminiferous tubules (Figures 1A and S1C) and the enrichment of marker genes in the corresponding subtypes (Figure S1D). Instead of relying on individual marker genes for subtype assignment, which may introduce biases (Figure S1E), our mapping approach considers the information from the whole transcriptome in each SPG subtype.

To spatially characterize the cell-cell communication landscape in SSC niches, we used the Slide-seq data to model the LR interactions among cell types by applying a spatial graph-based approach.[18] Briefly, the expression level of a LR pair between two neighboring cells was calculated by multiplying the ligand expression on the sending cell with the receptor expression on the neighboring receiving cell. The strength of a LR pair between two cell types was then calculated by summing the expression level of that LR pair between cell pairs that belong to the queried cell types (Figure 1B). Both the sender cells and the receiver cells contribute to the overall activity of a LR pair, and each cell is assigned with a value that represents its contribution to the activity of that LR pair. This value can then be plotted to visualize the spatial expression of the LR pair in the testis. For example, the GDNF and FGF-mediated LR interactions were found to be enriched at the basal compartment of seminiferous tubules where the SSCs reside (Figure S1F), consistent with known biology.[5,19,20]

Across a testis cross-section, unique associations between Sertoli cells and germ cells at specific stages of their development can be found in different seminiferous tubules. These cellular associations represent different stages within the cycle of the seminiferous epithelium.[21] To understand if and how the expression levels of LR pairs differ at various stages of the cycle of the seminiferous epithelium, we employed a previously established computational pipeline[15] to group cells belonging to the same seminiferous tubule (Figure S1G) and assign each seminiferous tubule to one of the four stage clusters (stages I–III, IV–VI, VII and VIII, and IX–XII) using the Slide-seq data (Figures 1C and S1H). Examination of the expression level of LR pairs such as the Gdnf-Gfr$\alpha$1 pair across stages suggests potential stage-specific expressions of certain LR pairs (Figure S1I). Indeed, we identified differentially expressed LR pairs across stages (Figure 1D). For example, LR pairs such as Gip-Tshr, Fgb-Tlr4, and S100a1-Tlr4 are enriched primarily in stage IV–VI tubules (Figure 1E), while Il16-Grin2d, Prss23-Tmem222, and Cdh6-Cntn1 are differentially expressed in stage I–III tubules (Figure S1J). Thus, our data systematically revealed variations in cell-cell communications during different developmental stages of spermatogenesis.

To gain a systematic understanding of the contribution of each testicular cell type in the regulation of SSC functions, we calculated the expression levels of LR pairs between cells in SPG1 (containing the SSCs) and each of their neighboring cell types. Cell type-specific LR interactions were identified (Figure 1F). For example, LR pairs Tfpi-Lrp1, Cd14-Itgb1, and Stab1-Ntm are enriched in the Leydig cell-SPG1 interaction (Figure 1G). To validate the result of this analysis, we focused on LR pair Cd14-Itgb1. We first confirmed the expression of *Cd14* in mouse Leydig cells by analyzing a public scRNA-seq dataset[16] (Figure S1K). Next, we performed multiplex single-molecule fluorescence *in situ* hybridization (smFISH) targeting *Cd14*, *Itgb1*, and Leydig cell marker *Cyp11a1* simultaneously. We found that, consistent with our analysis, *Cd14*-expressing Leydig cells localize near *Itgb1*-expressing SPG (Figure S1L).

### The PTN-mediated signaling in the mouse SSC niche

Among the LR-mediated signaling received by cells in SPG1, several PTN-mediated LR interactions were identified (Figures 2A and S2A). PTN is a heparin-binding growth factor that has been shown to regulate the self-renewal and retention of hematopoietic stem cells in the bone marrow vascular niche.[22] Furthermore, male mice over-expressed with a dominant-negative PTN mutant were sterile and had impaired spermatogenesis.[23] These observations prompted us to further investigate the functional roles of PTN in the SSC niche.

First, analysis of previous scRNA-seq datasets[16,24] showed that *Ptn* is expressed in the endothelial cells as well as the Leydig cells (albeit at a much lesser extent) in the mouse testis, whereas its expression is high in the Leydig cells, myoid cells, and Sertoli cells in the human testis (Figure S2B). Immunofluorescence (IF)

CellPress
OPEN ACCESS

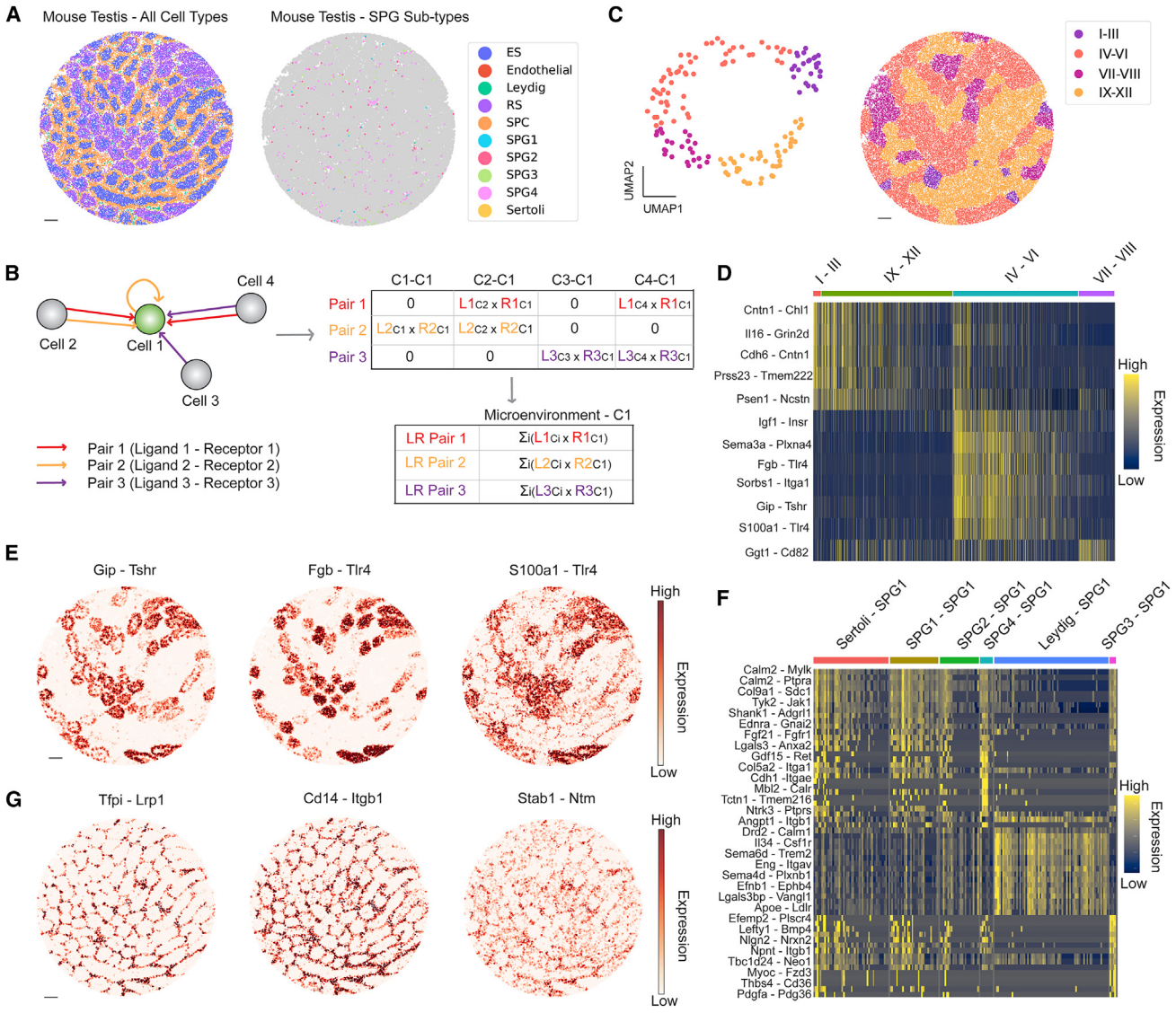


**Figure 1. A spatially resolved ligand-receptor (LR) interaction map of the mouse testis**

(A) Spatial mapping of major testicular cell types (left) and transcriptional states of spermatogonia (right) using a mouse testis Slide-seq dataset. ES, elongating/elongated spermatid; RS, round spermatid; SPC, spermatocyte; SPG, spermatogonium. Scale bar, 150 μm.

(B) Schematic of the method to calculate spatially resolved LR interactions between a set of cells. Cell-cell interactions are calculated by multiplying ligand expression on the sending cell with receptor expression on the neighboring receiving cell for each LR pair.

(C) Left: uniform manifold approximation and projection (UMAP) of seminiferous tubules in the transcriptome space colored by the stages of the cycle of the seminiferous epithelium. Right: spatial mapping of the stages of the cycle of the seminiferous epithelium. Scale bar, 150 μm.

(D) Differentially expressed LR pairs across the stages of the seminiferous epithelium cycle.

(E) Spatial expression patterns of selective LR pairs enriched in stages IV–VI of the seminiferous epithelium cycle. Scale bar, 160 μm.

(F) Differentially expressed LR pairs among cell type-SPG1 pairs. The heatmap shows 60 representative LR pairs. Every other row of the heatmap is labeled because of space limitations. The full list of LR pairs is provided in Table S1.

(G) Spatial expression patterns of selective LR pairs enriched in the Leydig cell-SPG1 pair. Scale bar, 160 μm.

analysis confirmed the expression of the PTN protein in the VWF$^+$ endothelial cells in the mouse testis (Figure 2B). Analysis of the mouse Slide-seq data (Figure S2C), multiplexed smFISH (Figure S2D), and IF analysis (Figure S2E) confirmed the expression of *Ptn* mRNA and protein in mouse Leydig cells.

Second, our LR interaction analysis showed that the PTN signaling can be mediated through SDC receptors expressed in SPG1 cells (Figure 2A). IF analysis confirmed the co-localization of the PTN protein with SDC4 at the surface of CDH1$^+$ mouse undifferentiated SPG (Figure 2C). Moreover, both the SDC4 protein and the PTN protein are present in GFRa1$^+$ undifferentiated SPG (Figures S2F–S2H).

Finally, to evaluate the functional impact of the PTN protein on SSCs, we performed the SSC transplantation assay

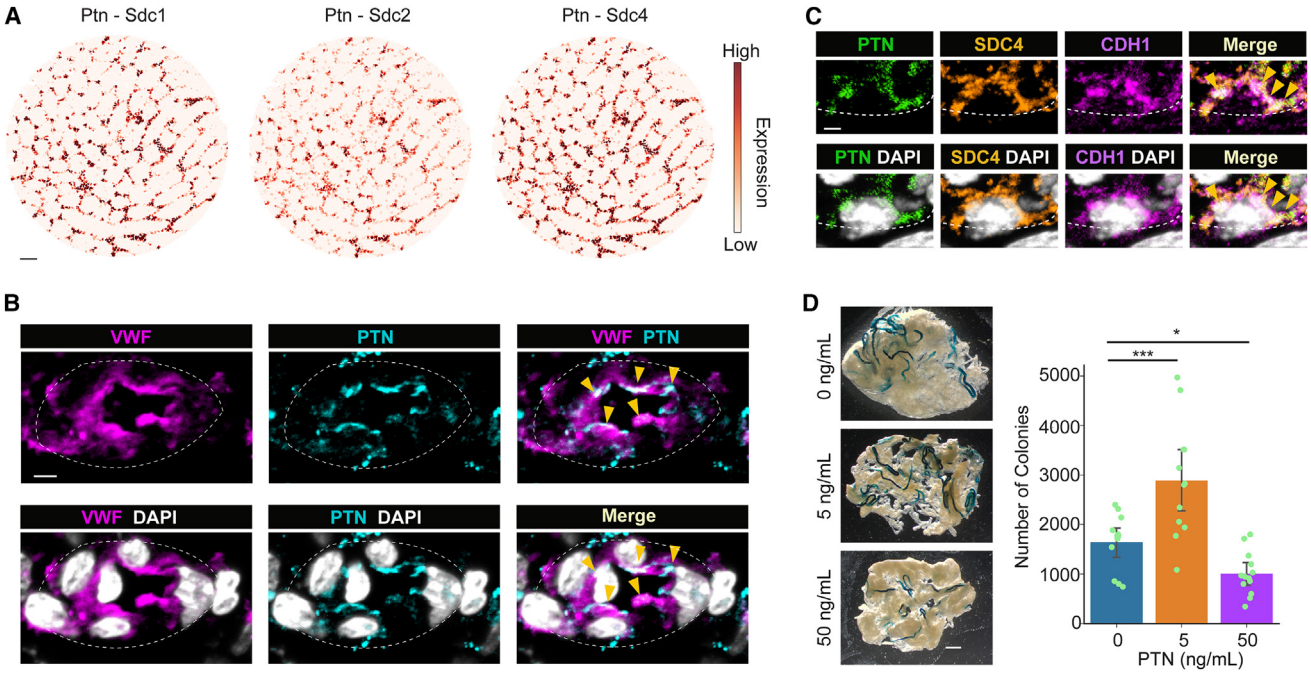


**Figure 2. PTN-mediated signaling regulates the functions of mouse SSCs**

(A) Spatial expression patterns of Ptn-Sdc pairs revealed by the mouse testis Slide-seq data. Scale bar, 160 μm.

(B) Endothelial cell marker protein VWF co-localizes with PTN protein (yellow arrowheads). The white dashed line outlines the blood vessel. Scale bar, 3 μm.

(C) Co-localization of PTN and SDC4 protein in a CDH1$^{+}$ undifferentiated spermatogonium (yellow arrowheads). The white dashed line outlines the basement membrane of the seminiferous tubule. Scale bar, 2 μm.

(D) Cultured mouse SSCs treated with PTN protein at 0, 5, or 50 ng/mL were transplanted into busulfan-treated recipients (n = 12, n = 12, and n = 13 recipient testes for the 0, 5, and 50 ng/mL group, respectively). Colony numbers in recipient testes were determined two months later using the LacZ staining. Colony counts were normalized as "per culture well" to make fair comparisons across groups. Data are represented as mean ± SD. One-way ANOVA followed by Fisher's least significant difference test; *$p < 0.05$ and ***$p < 0.001$. Representative images of the LacZ-stained recipient testes for each group are shown. Scale bar, 1 mm.

(STAR Methods). Donor SSCs treated with recombinant PTN protein at different concentrations (0, 5, and 50 ng/mL, respectively) together with recombinant GDNF and FGF2 protein were transplanted into busulfan-treated mouse testes. Two months later, we counted the number of colonies formed by the donor cells in each recipient testis. Compared with the 0 ng/mL PTN group, there was a significant increase in the number of colonies in the 5 ng/mL group (an average 76% increase). Intriguingly, the average number of colonies decreased by 39% in the 50 ng/mL group (Figure 2D). The average total number of cells harvested at the end of culture and used for the transplantation assay was $4.86 \times 10^5$, $5.74 \times 10^5$, and $4.11 \times 10^5$ per well for the 0, 5, and 50 ng/mL groups, respectively. Thus, the differences in the total number of cells per culture well between treatment groups cannot fully explain the differences we observed in the result of the transplantation assay. Moreover, fluorescence-activated cell sorting (FACS) analysis of the cultured SPG stained with different undifferentiated SPG markers (Gfra1, Cdh1, Thy1, and Itga6) and differentiation marker (Kit) showed no statistically significant differences between groups (Figures S2I and S2J). This suggests that PTN treatment *in vitro* affects the size of the colony in the transplantation assay, likely by changing the number of SSCs with colonization potential rather than influencing the percentage of the undifferentiated SPG in the cultured cells.

Together, our data suggest that in the mouse SSC niche, PTN protein secreted from the endothelial cells and Leydig cells regulates SSC functions at least partially through the SDC receptors.

## Global cell-cell communications in the mouse testis

To gain a global understanding of the cell-cell communication landscape in the mouse testis, LR pairs identified from the Slide-seq data were grouped into signaling pathways based on the curated LR information from the CellChatDB database.[25] Using an optimal transport-based approach,[26] we calculated the activities of each signaling pathway using the mouse Slide-seq datasets (STAR Methods). Across three replicates, we reproducibly identified signaling pathways with a high level of activities in the mouse testis such as the angiotensinogen (AGT) pathway (including LR pairs Agt-Agtr1a, Agt-Agtr1b, and Agt-Mas1), the FGF pathway (including Fgf2-Fgfr1, Fgf7-Fgfr3, Fgf10-Fgfr2, etc.), and the ADIPONECTIN pathway (including Adipoq-Adipor1 and Adipoq-Adipor2) (Figure 3A). Furthermore, we interpolated the spatial signaling direction of each pathway and showed that the activity of each signaling pathway was enriched in distinct tissue regions (Figure 3B).

Cell type-specific activity analysis identified signaling pathways differentially received by each testicular cell type (Figure 3C). For

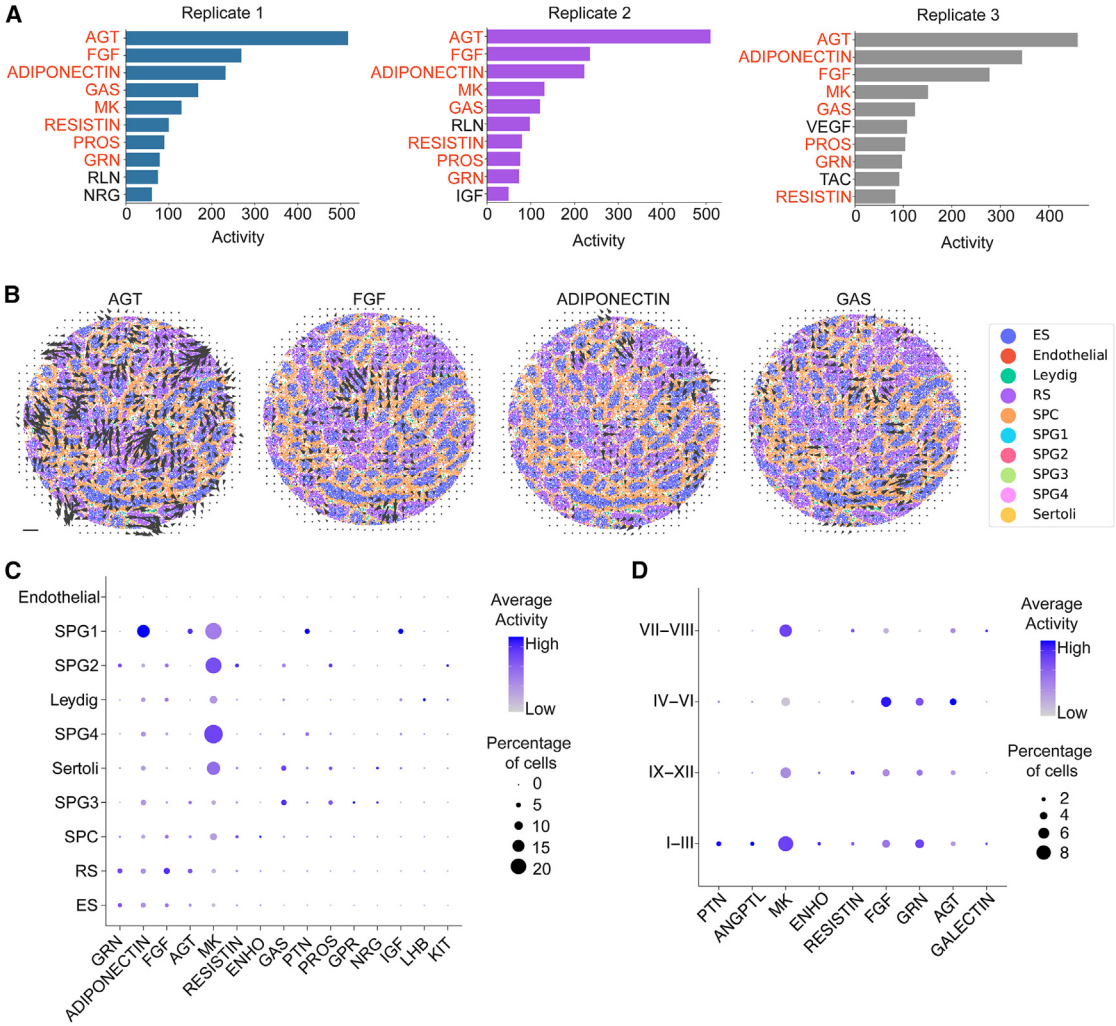


**Figure 3. Global signaling activities in the mouse testis**

(A) The top 10 signaling pathways with the highest activities across 3 replicates of mouse testis Slide-seq datasets. Pathways in red are shared across replicates.

(B) The signaling directions of four signaling pathways with high activities. The size of the arrow is proportional to the strength of the signaling activity. Scale bar, 200 μm.

(C) Dot plot showing the differential signaling activities received by each mouse testicular cell type.

(D) Dot plot showing the differential signaling activities received by cells in each stage of the cycle of the seminiferous epithelium.

example, the PTN pathway exerts the most of its effects on cells in SPG1 (Figure 3C), consistent with our analyses above. Furthermore, SPG1 is the main cell type to be influenced by the insulin-like growth factor (IGF)-mediated signaling (Figure 3C), corroborating the important roles of the IGF signaling in regulating mouse SSC functions.[27] Of interest, our analysis showed an enrichment of midkine (MK)-mediated signaling activity in SPG1, SPG2, SPG4, and Sertoli cells (Figure 3C). MK is a heparin-binding growth factor. Previous studies have revealed the functional roles of MK in promoting proliferation and self-renewal of embryonic stem cells[28] and in preventing hypoxia-induced apoptosis of mesenchymal stem cells.[29] Given that MK interacts with SDC receptors in the testis according to our spatial LR interaction map (Figure S2K), it is possible that MK-mediated signaling is involved in regulating SSC functions.

The non-random spatial activity patterns of the signaling pathways (Figure 3B) prompted us to investigate if their spatial distributions are related to the stages of the cycle of the seminiferous epithelium. Indeed, several signaling pathways with stage-specific activities were identified (Figure 3D). For instance, the MK signaling activity is enriched in the stage I–III and VII–VIII tubules, while the FGF and AGT signaling are preferentially activated in stage IV–VI tubules (Figure 3D).

## A spatially resolved LR interaction map of the human testis

A recent scRNA-seq study of the human testis identified five SPG subtypes that follow the order of SPG1 to SPG5 (corresponding to state 0 to state 4 in the original study) on the basis of transcriptional profiles and developmental trajectories of the

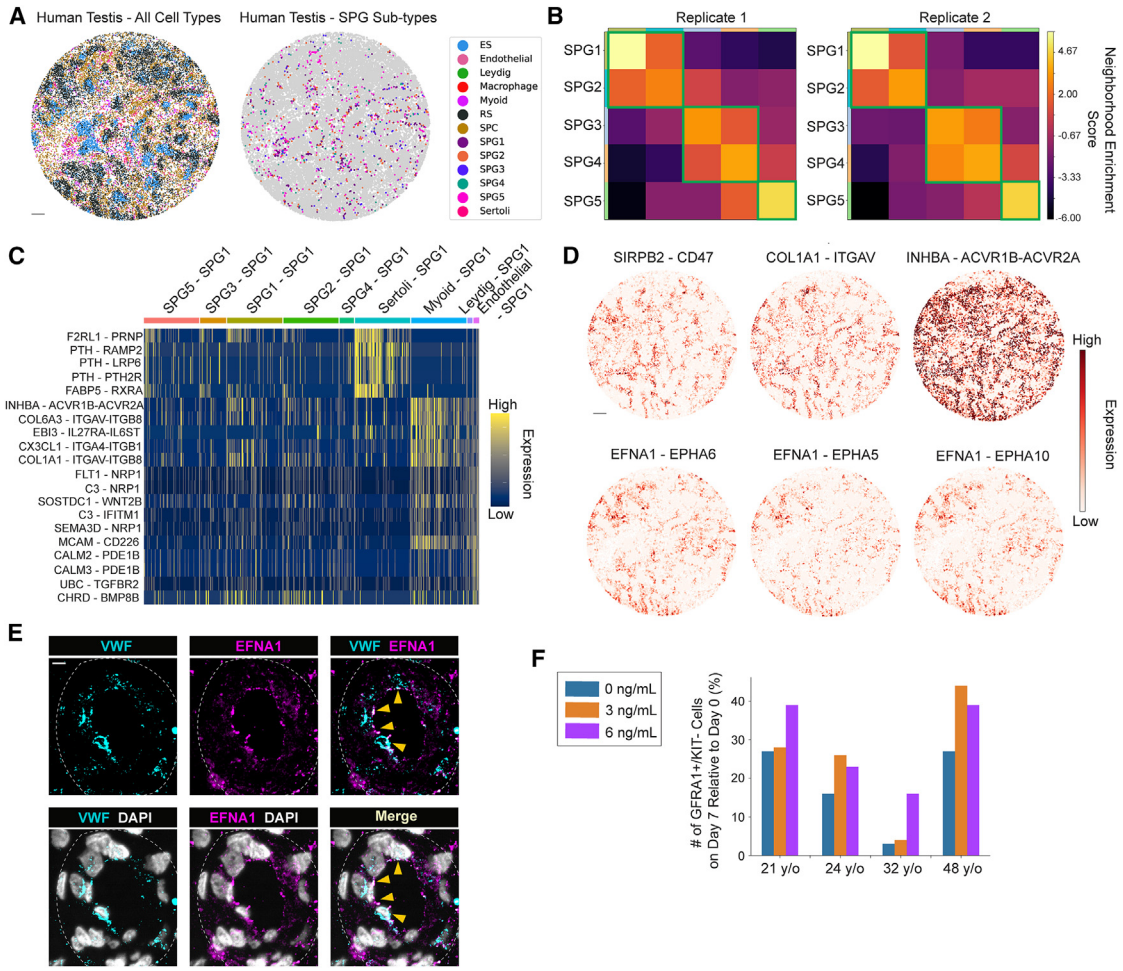


**Figure 4. A spatially resolved LR interaction map of the human testis**

(A) Spatial mapping of major testicular cell types (left) and transcriptional states of spermatogonia (right) in a human testis sample. ES, elongating/elongated spermatid; RS, round spermatid; SPC, spermatocyte; SPG, spermatogonium. Scale bar, 300 μm.

(B) The spatial relationship between the five SPG transcriptional subtypes as quantified by the neighborhood enrichment score in two independent human Slide-seq datasets.

(C) Differentially expressed LR pairs among SPG1-neighboring cell type pairs.

(D) Spatial expression patterns of selective LR pairs enriched in myoid cell-SPG1 (upper panel) and endothelial cell-SPG1 (lower panel) pairs. Scale bar, 320 μm.

(E) Protein expression of VWF and EFNA1 in a human testicular sample. The white dashed line outlines the blood vessel. Yellow arrowheads denote protein co-localization. Scale bar, 8 μm.

(F) Bar graph showing the number of GFRA1$^{+}$; KIT$^{-}$ human SPG on day 7 normalized against that from day 0. Cells were treated with recombinant human ENFA protein at 0, 3, and 6 ng/mL, respectively. Data from 4 patient samples are shown.

cells.[24] Using the same cell type deconvolution approach as the one applied to the mouse Slide-seq data,[17] we spatially mapped the human SPG subtypes using human Slide-seq datasets we have previously generated[15] (Figures 4A and S3A). Cells in SPG1 and SPG2 express known SSC markers such as *ID4* and *UTF1*, whereas known markers of differentiation (*KIT* and *STRA8*) or proliferation (*MKI67*) are mainly expressed during or after SPG3 (Figure S3B). Instead of relying on individual marker genes for subtype assignment which may introduce biases (Figure S3C), our mapping approach considers the information from the whole transcriptome in each SPG subtype. Interestingly, neighborhood enrichment analysis reproducibly identified three spatial clusters within the human SPG subtypes: (1) cells in SPG1 and SPG2, (2) cells in SPG3 and SPG4, and (3) cells in SPG5 (Figure 4B). Such a pattern of spatial separation was not observed in the mouse SPG subtypes (Figure S3D).

Next, we established a LR interaction map in the human testis using the same method that we have used for the mouse testis Slide-seq data. To gain a systematic understanding of the contribution of each testicular cell type in the regulation of SSC functions, we calculated the expression levels of LR pairs between cells in SPG1 and each of their neighboring cell types, respectively. Cell type-specific LR interactions were identified (Figure 4C). For example, LR pairs SIRPB2-CD47, COL1A1-ITGAV,

and INHBA-ACVR1B-ACVR2A are enriched in the myoid cell-SPG1 interaction (Figure 4D, upper panel).

Importantly, we observed an enrichment of several ephrin A1 (EFNA1)-ephrin type A receptor (EPHA) pairs between the endothelial cells and the cells in SPG1 in the Slide-seq data (Figure 4D, lower panel). EPHA2 has been previously shown as a critical modifier of self-renewal signals in mouse SSCs.[30] However, if and how the ephrin signaling is involved in regulating the functions of human SSCs remain unclear. IF analysis identified EFNA1 protein in VWF$^+$ endothelial cells in the human testis (Figure 4E). To further investigate the function of EFNA1, cultured ITGA6$^+$ human SPG were treated with recombinant human EFNA1 proteins at 0, 3, and 6 ng/mL, respectively (Figure S3E). Using FACS analysis, we observed a decrease in the total number of cells, including the GFRa1$^+$; KIT$^-$ undifferentiated SPG, in each culture well across treatment groups after 7 days of culture compared with day 0 (Figure S3F). However, there was a consistent trend across 4 replicates in which more viable cells (Figures S3G and S3H, top row) and more GFRa1$^+$; KIT$^-$ undifferentiated SPG (Figures 4F and S3H, bottom row) were retained in the 3 and 6 ng/mL EFNA1 groups compared with the 0 ng/mL group. Moreover, no consistent trend was observed for the number of KIT$^+$ differentiating SPG (including GFRa1$^-$; KIT$^+$ and GFRa1$^+$; KIT$^+$) across replicates (data not shown). Although the increase in the retainment of total number of viable cells and the number of GFRa1$^+$; KIT$^-$ undifferentiated SPG in the 3 and 6 ng/mL EFNA1 groups is not statistically significant, because of high variance among patient samples ($p > 0.05$, one-way ANOVA) (Figure S3I), the consistent trend across 4 replicates suggests that EFNA1 produced by the endothelial cells might play a role in regulating human SSC functions.

## Global cell-cell communications in the human testis

Using the same optimal transport-based approach applied to the mouse Slide-seq data,[26] we grouped LR pairs into signaling pathways and calculated their activities using the human Slide-seq datasets. Consistent with our observations in the mouse data, several signaling pathways such as the PTN-, MK-, and FGF-mediated signaling show strong activities in the human testis (Figure S3J). Surprisingly, some signaling pathways which show high levels of activities in the mouse testis such as the AGT pathway and the ADIPONECTIN pathway (Figure 3A), exhibit no or limited activities in the human testis (Figure S3J). These findings demonstrate the convergent and divergent aspects of signaling activities between the mouse and human spermatogenesis.

Next, we interpolated the spatial signaling direction of pathways and showed that their activities are enriched in distinct tissue regions (Figure S3K). Cell type-specific activity analysis identified signaling pathways differentially received by each testicular cell type (Figure S3L). For example, the FGF pathway exerts the most of its effects on cells in SPG1 and SPG2 (Figure S3L), consistent with a prior observation.[31] We also found that myoid cells are the major cell type to receive the signaling activities of the PDGF pathway (including LR pairs PDGFA-PDGFRA, PDGFA-PDGFRB, etc.) and VISFATIN pathway (NAMPT-INSR and NAMPT-ITGA5-ITGB1), while Sertoli cells receive the most of GAS (GAS6-AXL, GAS6-MERTK, and GAS6-TYRO3) signaling activities (Figure S3L).

## Disruptions in the spatial expression patterns of LR pairs induced by diabetes

We recently demonstrated that spatial transcriptomics can be applied to characterize pathological changes in spermatogenesis.[15] We revealed a disruption in the spatial organization of testicular cell types in leptin-deficient diabetic mice (*ob/ob*) compared with the WT[15] (Figure 5A).

To further characterize the pathological changes of *ob/ob* testes at the molecular level, we devised a spatial autocorrelation score to quantify the spatial expression pattern of a given LR pair (STAR Methods). A high spatial autocorrelation score represents a non-random spatial distribution of LR expression, whereas a low score suggests a distribution without a clear spatial pattern. By calculating the spatial autocorrelation score for each LR pair using Slide-seq data from both the WT and *ob/ob* mice, we identified LR pairs with significantly lower scores in the *ob/ob* testes than in the WT ($p < 0.05$, Wilcoxon rank-sum test) (Figure 5B; Table S2). Visualization of some of the identified LR pairs clearly showed changes in their spatial expression patterns in the *ob/ob* sample compared with the WT (Figure 5C). For example, in the WT testis, the expressions of LR pairs Adam12-Itga3 and Ebi3-Il6st are spatially enriched at the basal compartment of seminiferous tubules where the SSCs reside. However, their spatial expressions become "diffused" in the *ob/ob* testis (Figure 5C).

To validate the results revealed by the spatial autocorrelation score analysis, we applied SPARK,[32] a generalized linear spatial model, to statistically test if the spatial expression of a given LR pair is non-random within a seminiferous tubule. We reasoned that the alteration in the spatial expression of LR pairs revealed by the spatial autocorrelation score analysis may be reflected at the level of individual seminiferous tubules. To this end, we looked for the edge cases where a given LR pair shows a statistically significant non-random spatial distribution in the WT tubules but entirely loses its specialized spatial expression patten in *ob/ob* tubules. We applied SPARK to 6 LR pairs whose spatial autocorrelation scores significantly decrease in *ob/ob vs.* WT tubules (shown in Figures 5B and 5C). We found that 4 of the LR pairs (F13a1-Itga9, Lnx1-Igsf5, Serpine1-Sele, and Ebi3-Il6st) passed the stringent statistical test of SPARK ($n = 25$ seminiferous tubules tested) (Figure S4A). The alterations in the spatial expression patterns of the remaining two LR pairs (Adam12-Itga3 and Col1a1-Cd93) are likely not drastic enough to be characterized as a total loss of spatial patterns by SPARK. This analysis suggests that the spatial autocorrelation score analysis captures real changes in the spatial expression pattens of LR pairs. Because not all LR pairs show changes in their spatial distribution drastic enough to be captured by SPARK, we argue that the spatial autocorrelation score is a more sensitive approach to detect global spatial re-distribution of LR pair expression.

Of note, the alterations in spatial expression patterns of the LR pairs are not likely a byproduct of the changes in cellular organizations in the *ob/ob* testis. This is because out of all the LR pairs quantified, ~95% (564 of 594) showed no or limited alterations in

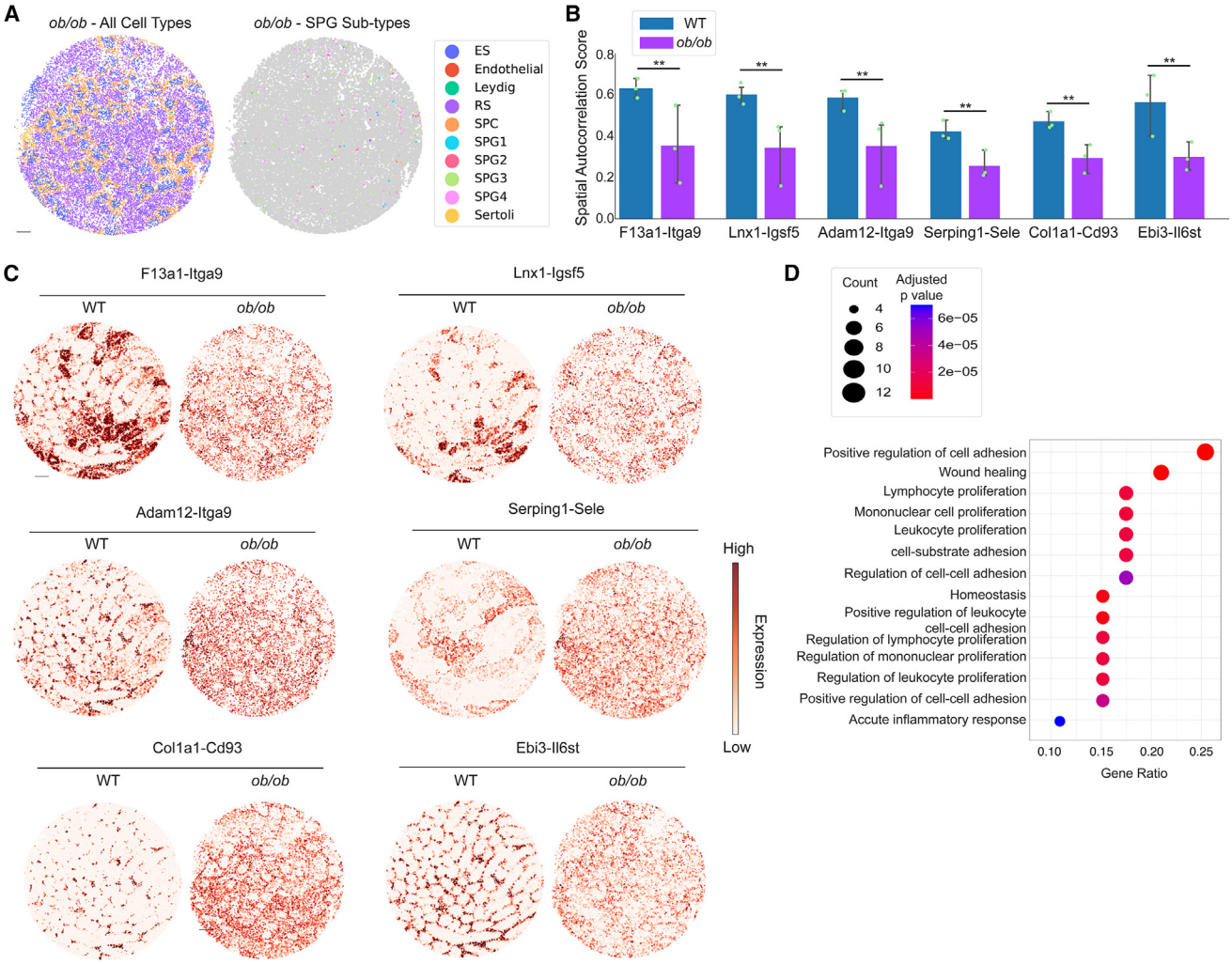


**Figure 5. Diabetes causes disruptions in spatial expression patterns of selective LR pairs**

(A) Spatial mapping of major mouse testicular cell types (left) and transcriptional states of spermatogonia (right) in an *ob/ob* testis sample. ES, elongating/elongated spermatid; RS, round spermatid; SPC, spermatocyte; SPG, spermatogonium. Scale bar, 300 μm.

(B) The spatial expression patterns of selective LR pairs as quantified by the spatial autocorrelation score in both WT and *ob/ob* testis samples. **$p < 0.01$ (Wilcoxon rank-sum test). n = 3 replicates in each group. Data are represented as mean ± SD.

(C) Visualization of the spatial expression patterns of the LR pairs quantified in (B) in both WT and *ob/ob* testis samples. Scale bar, 350 μm.

(D) Gene Ontology analysis of LR pairs with disrupted spatial expression patterns in *ob/ob* testis samples.

their spatial expression patterns (Figures S4B and S4C). This suggests that only a specific subset of LR pairs is affected under the diabetic condition. To reveal the functions of the affected LR pairs, Gene Ontology (GO) enrichment analysis was performed. We found that the affected LR pairs are enriched in signaling pathways related to cell adhesion and immune-related cell proliferation (Figure 5D). Together, our data implies that a spatial re-distribution of LR pairs involved in inflammatory responses underlies diabetes-induced testicular injuries.

## DISCUSSION

The stem cell niche represents a unique tissue microenvironment, in which cellular components of the niche interact with the stem cells to maintain the self-renewal of the stem cells or promote their differentiation. A large portion of these cellular interactions are mediated through LR pairs. Knowledge of these LR interactions has practical implications, as the regenerative potential of tissue-specific stem cells can be exploited therapeutically.[33]

Understanding how the niche controls the stem cell phenotype through LR interactions represents a formidable challenge because of the complexity of the niche composition, its dynamics, and nonlinear stem cell-niche interactions. To overcome this challenge, we have used spatial transcriptomics and computational approaches to systematically map the LR interaction landscape of the mammalian SSC niche. To increase the accessibility of our datasets to the whole research community,

we have established an interactive data visualization portal using the framework of Single Cell Portal (Portal ID: SCP2166) for the purpose of data visualization and exploration. Users could simply type in a gene name to search for a LR pair of interest and visualize its spatial distribution.

Unlike the studies using scRNA-seq in which LR pairs were inferred between every pair of cells regardless of their spatial distance in the tissue, we used a spatial graph-based network to extract LR pairs only from cells within biologically meaningful distances. This approach significantly reduces the number of false-positive LR pairs while preserving information of the key niche factors. Using this approach, we identified cell type-specific LR interactions in the SSC niches. The spatial information obtained from Slide-seq also enabled the classification of stages of the cycle of seminiferous epithelium, facilitating the identification of stage-specific LR expressions.

Among the ligands identified from our systematic approach, PTN may serve as a key niche factor in regulating the functions of mouse SSCs through SDC receptors. Indeed, the transplantation assay showed that PTN exerts a dose-dependent biphasic effect on SSCs where PTN at 5 ng/mL promotes SSC colonization, whereas PTN at 50 ng/mL suppresses it. Given that cells treated with PTN were cultured in medium supplemented with FGF2 and that SDC receptors on the surface of SSCs can also bind to FGFs,[9] it is possible that PTN at 50 ng/mL competes with FGF2 for SDC receptor binding, therefore inhibiting the self-renewal signal induced by FGF2. Additional support for our competitive binding hypothesis comes from a previous observation that male mice over-expressing a dominant-negative mutant of PTN were sterile with a diminished spermatogonial pool.[23] This mutant PTN contains only the first N-terminal 40 amino acids (aa) of PTN, including a 32 aa signal peptide and a sequence of GKKEKPEK. The presence of the signal peptide and the highly positively charged Lysine residues means that this PTN mutant can be secreted and interact with numerous SSC cell surface receptors that have an affinity for positively charged molecules, including the SDC receptors. Therefore, overexpression of this mutant PTN may cause sterility through competing with FGFs for receptor binding on the surface of SSCs. Future studies using neutralizing antibodies against PTN and PTN knockout mice are needed to reveal the mechanisms underlying the observed impact of PTN on mouse SSCs.

In the human testis, we identified EFNA1 as a potential niche factor to regulate SSC functions. We found that the number of GFRA1$^+$; KIT$^-$ undifferentiated SPG decreased over 7 days in culture across all the treatment groups. However, there was a consistent trend (across 4 replicate human testis samples) showing that EFNA1 treatment improved the retention of GFRA1$^+$; KIT$^-$ undifferentiated SPG in culture compared with the untreated group. This increase in the retainment of GFRA1$^+$; KIT$^-$ SPG by EFNA1 is not statistically significant, likely because of high variance in human samples. In addition, FGF2 has been shown to induce the expression of EFNA1 receptor EPHA2 and EPHA2 phosphorylation in the absence of EFNA1 in the cultured mouse SPG.[30] Therefore, it is possible that FGF2 in the culture medium partially offsets the effects of EFNA1 treatment on human SSCs. Nonetheless, the consistent trend of an improved retention of human GFRA1$^+$; KIT$^-$ undifferentiated SPG by EFNA1 treatment across 4 highly heterogeneous human testis samples suggests a potential functional role of EFNA1 on human SSCs.

Another advantage of our approach is to enable systematic characterizations of signaling pathways inferred from individual LR pairs in a spatially resolved manner. Taking into account the spatial localizations of sender cells and receiver cells, we were able to pinpoint both the activity and the direction of each signaling pathway across the tissue sections. In turn, this facilitated the identification of signaling pathways with cell type specificity or stage specificity.

Finally, we demonstrated the strengths of our approach to profile pathological conditions. By quantifying the spatial expression pattern of each LR pair and observing how its spatial pattern changes under the diabetic condition compared with the WT, we systematically identified LR pairs susceptible to diabetes. Given that the number of affected LR pairs (~5%) is relatively small compared with the total number of LR pairs profiled, the changes in their spatial expression patterns are unlikely a result of a disruption in tissue structures in general. Thus, the spatial redistribution of this selected subset of LR pairs may be a potential cause to the diabetes-induced testicular injuries. This work demonstrates how cell-cell communications alter in a disease state. We anticipate that this approach can be widely adapted to examine tissue microenvironments under various disease states, such as cardiovascular diseases and cancer.

In summary, we established an innovative approach to comprehensively reveal the detailed cell-cell communication landscape that instructs SSC functions in both the mouse and the human testis. This ability to profile systematically, quantitatively, and in a spatially resolved manner the tissue-wide LR interaction landscape as well as signaling pathway activities at high cellular resolution may have a transformative potential in the field of stem cell biology and beyond.

## Limitations of the study

Although Slide-seq provides a high spatial resolution (10 μm), it is possible that one Slide-seq bead could capture mRNA from 2 to 3 adjacent cells from different cell types. Thus, this intrinsic limitation of Slide-seq means that the resulting data does not represent authentic single-cell level transcriptome. However, our cell type assignment approach based off on RCTD[17] effectively addresses this challenge by deconvoluting the transcriptome profile captured by each bead. Yet the accuracy of cell type assignment would likely further benefit from an enhanced capture efficiency of testicular mRNA by the Slide-seq array, especially for the assignment of SPG subtypes. A low RNA capture rate also means that lowly expressed genes might be overlooked, leading to the possibility that certain LR interactions might not be identified in the current study. In addition, our computational approach to infer signaling activities considers all cells across the testis. Future work that allows region-specific activity inference would pinpoint signaling pathways that are specifically active at the SSC niche more efficiently. Finally, spatial transcriptomics data alone does not directly represent protein abundance and cannot capture protein-specific modifications, such as protein phosphorylation,

glycosylation, and dimerization. A multimodal spatial omics profiling technology that combines protein and RNA readout may help address this challenge and further reduce the false-positive rate of LR pair identification.

## STAR★METHODS

Detailed methods are provided in the online version of this paper and include the following:

- KEY RESOURCES TABLE
- RESOURCE AVAILABILITY
  - Lead contact
  - Materials availability
  - Data and code availability
- EXPERIMENTAL MODEL AND STUDY PARTICIPANT DETAILS
  - Animals
  - Human samples
  - Primary cell cultures
- METHOD DETAILS
  - Slide-seq workflow
  - Immunofluorescence
  - smFISH
  - Culture of mouse spermatogonia for the transplantation assay
  - Transplantation assay
  - Isolation of human spermatogonia and culture
  - Multiparameter FACS
  - Computational methods for slide-seq data
  - Cell type assignment
  - Assignment of stages of the cycle of the seminiferous epithelium
  - Generation of a spatially resolved LR interaction map
  - Calculation of signaling activities and signaling directions
  - Neighborhood enrichment analysis
  - Calculation of the spatial autocorrelation score
  - Validation of the spatial autocorrelation score analysis
  - GO analysis
- QUANTIFICATION AND STATISTICAL ANALYSIS

## SUPPLEMENTAL INFORMATION

Supplemental information can be found online at https://doi.org/10.1016/j.celrep.2023.112737.

## ACKNOWLEDGMENTS

We thank Dylan Cable for discussions on using RCTD and Fei Chen for providing the Slide-seq arrays. H.C. acknowledges support from the NIH (R21HD110878) and the Cecil H. and Ida Green Center for Reproductive Biology Sciences Endowment. M.N. is supported by project grants from the CIHR (Canadian Institutes of Health Research) (PJT-156305 and PJT 153233). E.J.G. is supported by a Cancer Prevention & Research Institute of Texas Recruitment of First-Time, Tenure-Track Faculty Member Award (grant RR210077) and by the Cecil H. and Ida Green Center for Reproductive Biology Sciences.

## AUTHOR CONTRIBUTIONS

H.C. conceived and supervised the project. H.C., M.N., and K.E.O. designed experiments. H.C., S.R., Xin Zhang, Q.C., A.L.C.-B., Xiangfan Zhang, Y.S., and M.N. performed experiments. H.C., S.R., Xin Zhang, Q.C., A.C., Xiangfan Zhang, Y.S., and M.N. performed data analysis. K.E.O. provided human testicular samples. M.E., O.B., E.J.G., M.N., and K.E.O. provided consultations. H.C. wrote the manuscript with input from all authors.

## DECLARATION OF INTERESTS

The authors declare no competing interests.

Received: February 9, 2023
Revised: May 7, 2023
Accepted: June 19, 2023

## REFERENCES

1. de Rooij, D.G. (2017). The nature and dynamics of spermatogonial stem cells. Development *144*, 3022–3030. https://doi.org/10.1242/dev.146571.
2. Phillips, B.T., Gassei, K., and Orwig, K.E. (2010). Spermatogonial stem cell regulation and spermatogenesis. Philos. Trans. R. Soc. Lond. B Biol. Sci. *365*, 1663–1678. https://doi.org/10.1098/rstb.2010.0026.
3. Kubota, H., and Brinster, R.L. (2018). Spermatogonial stem cells. Biol. Reprod. *99*, 52–74. https://doi.org/10.1093/biolre/ioy077.
4. Yoshida, S., Sukeno, M., and Nabeshima, Y.I. (2007). A vasculature-associated niche for undifferentiated spermatogonia in the mouse testis. Science *317*, 1722–1726. https://doi.org/10.1126/science.1144885.
5. Meng, X., Lindahl, M., Hyvönen, M.E., Parvinen, M., de Rooij, D.G., Hess, M.W., Raatikainen-Ahokas, A., Sainio, K., Rauvala, H., Lakso, M., et al. (2000). Regulation of cell fate decision of undifferentiated spermatogonia by GDNF. Science *287*, 1489–1493. https://doi.org/10.1126/science.287.5457.1489.
6. Bhang, D.H., Kim, B.J., Kim, B.G., Schadler, K., Baek, K.H., Kim, Y.H., Hsiao, W., Ding, B.S., Rafii, S., Weiss, M.J., et al. (2018). Testicular endothelial cells are a critical population in the germline stem cell niche. Nat. Commun. *9*, 4379. https://doi.org/10.1038/s41467-018-06881-z.
7. Busada, J.T., and Geyer, C.B. (2016). The Role of Retinoic Acid (RA) in Spermatogonial Differentiation. Biol. Reprod. *94*, 10. https://doi.org/10.1095/biolreprod.115.135145.
8. Griswold, M.D., and Hogarth, C. (2018). Beyond stem cells: Commitment of progenitor cells to meiosis. Stem Cell Res. *27*, 169–171. https://doi.org/10.1016/j.scr.2018.01.032.
9. Kitadate, Y., Jörg, D.J., Tokue, M., Maruyama, A., Ichikawa, R., Tsuchiya, S., Segi-Nishida, E., Nakagawa, T., Uchida, A., Kimura-Yoshida, C., et al. (2019). Competition for Mitogens Regulates Spermatogenic Stem Cell Homeostasis in an Open Niche. Cell Stem Cell *24*, 79–92.e6. https://doi.org/10.1016/j.stem.2018.11.013.
10. Takashima, S., Kanatsu-Shinohara, M., Tanaka, T., Morimoto, H., Inoue, K., Ogonuki, N., Jijiwa, M., Takahashi, M., Ogura, A., and Shinohara, T. (2015). Functional differences between GDNF-dependent and FGF2-dependent mouse spermatogonial stem cell self-renewal. Stem Cell Rep. *4*, 489–502. https://doi.org/10.1016/j.stemcr.2015.01.010.
11. Shami, A.N., Zheng, X., Munyoki, S.K., Ma, Q., Manske, G.L., Green, C.D., Sukhwani, M., Orwig, K.E., Li, J.Z., and Hammoud, S.S. (2020). Single-Cell RNA Sequencing of Human, Macaque, and Mouse Testes Uncovers Conserved and Divergent Features of Mammalian Spermatogenesis. Dev. Cell *54*, 529–547.e12. https://doi.org/10.1016/j.devcel.2020.05.010.
12. Zhang, W., Xia, S., Xiao, W., Song, Y., Tang, L., Cao, M., Yang, J., Wang, S., Li, Z., Xu, C., et al. (2022). A single-cell transcriptomic landscape of mouse testicular aging. J. Adv. Res. https://doi.org/10.1016/j.jare.2022.12.007.

13. Jan, S.Z., Vormer, T.L., Jongejan, A., Röling, M.D., Silber, S.J., de Rooij, D.G., Hamer, G., Repping, S., and van Pelt, A.M.M. (2017). Unraveling transcriptome dynamics in human spermatogenesis. Development *144*, 3659–3673. https://doi.org/10.1242/dev.152413.

14. Shalek, A.K., and Satija, R. (2015). MERFISHing for spatial context. Trends Immunol. *36*, 390–391. https://doi.org/10.1016/j.it.2015.05.002.

15. Chen, H., Murray, E., Sinha, A., Laumas, A., Li, J., Lesman, D., Nie, X., Hotaling, J., Guo, J., Cairns, B.R., et al. (2021). Dissecting mammalian spermatogenesis using spatial transcriptomics. Cell Rep. *37*, 109915. https://doi.org/10.1016/j.celrep.2021.109915.

16. Green, C.D., Ma, Q., Manske, G.L., Shami, A.N., Zheng, X., Marini, S., Moritz, L., Sultan, C., Gurczynski, S.J., Moore, B.B., et al. (2018). A Comprehensive Roadmap of Murine Spermatogenesis Defined by Single-Cell RNA-Seq. Dev. Cell *46*, 651–667.e10. https://doi.org/10.1016/j.devcel.2018.07.025.

17. Cable, D.M., Murray, E., Zou, L.S., Goeva, A., Macosko, E.Z., Chen, F., and Irizarry, R.A. (2022). Robust decomposition of cell type mixtures in spatial transcriptomics. Nat. Biotechnol. *40*, 517–526. https://doi.org/10.1038/s41587-021-00830-w.

18. Raredon, M.S.B., Yang, J., Kothapalli, N., Lewis, W., Kaminski, N., Niklason, L.E., and Kluger, Y. (2023). Comprehensive visualization of cell-cell interactions in single-cell and spatial transcriptomics with NICHES. Bioinformatics *39*, btac775. https://doi.org/10.1093/bioinformatics/btac775.

19. Wright, W.W. (2022). The Regulation of Spermatogonial Stem Cells in an Adult Testis by Glial Cell Line-Derived Neurotrophic Factor. Front. Endocrinol. *13*, 896390. https://doi.org/10.3389/fendo.2022.896390.

20. Kubota, H., Avarbock, M.R., and Brinster, R.L. (2004). Growth factors essential for self-renewal and expansion of mouse spermatogonial stem cells. Proc. Natl. Acad. Sci. USA *101*, 16489–16494. https://doi.org/10.1073/pnas.0407063101.

21. Hess, R.A., and Renato de Franca, L. (2008). Spermatogenesis and cycle of the seminiferous epithelium. Adv. Exp. Med. Biol. *636*, 1–15. https://doi.org/10.1007/978-0-387-09597-4_1.

22. Himburg, H.A., Harris, J.R., Ito, T., Daher, P., Russell, J.L., Quarmyne, M., Doan, P.L., Helms, K., Nakamura, M., Fixsen, E., et al. (2012). Pleiotrophin regulates the retention and self-renewal of hematopoietic stem cells in the bone marrow vascular niche. Cell Rep. *2*, 964–975. https://doi.org/10.1016/j.celrep.2012.09.002.

23. Zhang, N., Yeh, H.J., Zhong, R., Li, Y.S., and Deuel, T.F. (1999). A dominant-negative pleiotrophin mutant introduced by homologous recombination leads to germ-cell apoptosis in male mice. Proc. Natl. Acad. Sci. USA *96*, 6734–6738. https://doi.org/10.1073/pnas.96.12.6734.

24. Guo, J., Grow, E.J., Mlcochova, H., Maher, G.J., Lindskog, C., Nie, X., Guo, Y., Takei, Y., Yun, J., Cai, L., et al. (2018). The adult human testis transcriptional cell atlas. Cell Res. *28*, 1141–1157. https://doi.org/10.1038/s41422-018-0099-2.

25. Jin, S., Guerrero-Juarez, C.F., Zhang, L., Chang, I., Ramos, R., Kuan, C.H., Myung, P., Plikus, M.V., and Nie, Q. (2021). Inference and analysis of cell-cell communication using CellChat. Nat. Commun. *12*, 1088. https://doi.org/10.1038/s41467-021-21246-9.

26. Cang, Z., Zhao, Y., Almet, A.A., Stabell, A., Ramos, R., Plikus, M.V., Atwood, S.X., and Nie, Q. (2023). Screening cell-cell communication in spatial transcriptomics via collective optimal transport. Nat. Methods *20*, 218–228. https://doi.org/10.1038/s41592-022-01728-4.

27. Huang, Y.H., Chin, C.C., Ho, H.N., Chou, C.K., Shen, C.N., Kuo, H.C., Wu, T.J., Wu, Y.C., Hung, Y.C., Chang, C.C., and Ling, T.Y. (2009). Pluripotency of mouse spermatogonial stem cells maintained by IGF-1- dependent pathway. Faseb. J. *23*, 2076–2087. https://doi.org/10.1096/fj.08-121939.

28. Yao, X., Tan, Z., Gu, B., Wu, R.R., Liu, Y.K., Dai, L.C., and Zhang, M. (2010). Promotion of self-renewal of embryonic stem cells by midkine. Acta Pharmacol. Sin. *31*, 629–637. https://doi.org/10.1038/aps.2010.39.

29. Zhao, S.L., Zhang, Y.J., Li, M.H., Zhang, X.L., and Chen, S.L. (2014). Mesenchymal stem cells with overexpression of midkine enhance cell survival and attenuate cardiac dysfunction in a rat model of myocardial infarction. Stem Cell Res. Ther. *5*, 37. https://doi.org/10.1186/scrt425.

30. Morimoto, H., Kanatsu-Shinohara, M., Orwig, K.E., and Shinohara, T. (2020). Expression and functional analyses of ephrin type-A receptor 2 in mouse spermatogonial stem cells. Biol. Reprod. *102*, 220–232. https://doi.org/10.1093/biolre/ioz156.

31. Mirzapour, T., Movahedin, M., Tengku Ibrahim, T.A., Koruji, M., Haron, A.W., Nowroozi, M.R., and Rafieian, S.H. (2012). Effects of basic fibroblast growth factor and leukaemia inhibitory factor on proliferation and short-term culture of human spermatogonial stem cells. Andrologia *44* (*Suppl 1*), 41–55. https://doi.org/10.1111/j.1439-0272.2010.01135.x.

32. Sun, S., Zhu, J., and Zhou, X. (2020). Statistical analysis of spatial expression patterns for spatially resolved transcriptomic studies. Nat. Methods *17*, 193–200. https://doi.org/10.1038/s41592-019-0701-7.

33. Wagers, A.J. (2012). The stem cell niche in regenerative medicine. Cell Stem Cell *10*, 362–369. https://doi.org/10.1016/j.stem.2012.02.018.

34. Stickels, R.R., Murray, E., Kumar, P., Li, J., Marshall, J.L., Di Bella, D.J., Arlotta, P., Macosko, E.Z., and Chen, F. (2021). Highly sensitive spatial transcriptomics at near-cellular resolution with Slide-seqV2. Nat. Biotechnol. *39*, 313–319. https://doi.org/10.1038/s41587-020-0739-1.

35. Yeh, J.R., Zhang, X., and Nagano, M.C. (2007). Establishment of a short-term in vitro assay for mouse spermatogonial stem cells. Biol. Reprod. *77*, 897–904. https://doi.org/10.1095/biolreprod.107.063057.

36. Himburg, H.A., Muramoto, G.G., Daher, P., Meadows, S.K., Russell, J.L., Doan, P., Chi, J.T., Salter, A.B., Lento, W.E., Reya, T., et al. (2010). Pleiotrophin regulates the expansion and regeneration of hematopoietic stem cells. Nat. Med. *16*, 475–482. https://doi.org/10.1038/nm.2119.

37. Nagano, M., Avarbock, M.R., and Brinster, R.L. (1999). Pattern and kinetics of mouse donor spermatogonial stem cell colonization in recipient testes. Biol. Reprod. *60*, 1429–1436. https://doi.org/10.1095/biolreprod60.6.1429.

38. Ogawa, T., Aréchaga, J.M., Avarbock, M.R., and Brinster, R.L. (1997). Transplantation of testis germinal cells into mouse seminiferous tubules. Int. J. Dev. Biol. *41*, 111–122.

39. Nagano, M.C., and Yeh, J.R. (2011). The Cluster-Forming Activity Assay: A Short-Term In Vitro Method to Analyze the Activity of Mouse Spermatogonial Stem Cells. Stem Cell Biol. Res. *125*, 125–134. https://doi.org/10.1007/978-1-61737-973-4_6.

40. Murdock, M.H., David, S., Swinehart, I.T., Reing, J.E., Tran, K., Gassei, K., Orwig, K.E., and Badylak, S.F. (2019). Human Testis Extracellular Matrix Enhances Human Spermatogonial Stem Cell Survival In Vitro. Tissue Eng. *25*, 663–676. https://doi.org/10.1089/ten.TEA.2018.0147.

41. Dobin, A., Davis, C.A., Schlesinger, F., Drenkow, J., Zaleski, C., Jha, S., Batut, P., Chaisson, M., and Gingeras, T.R. (2013). STAR: ultrafast universal RNA-seq aligner. Bioinformatics *29*, 15–21. https://doi.org/10.1093/bioinformatics/bts635.

42. Hafemeister, C., and Satija, R. (2019). Normalization and variance stabilization of single-cell RNA-seq data using regularized negative binomial regression. Genome Biol. *20*, 296. https://doi.org/10.1186/s13059-019-1874-1.

43. Johnston, D.S., Wright, W.W., Dicandeloro, P., Wilson, E., Kopf, G.S., and Jelinsky, S.A. (2008). Stage-specific gene expression is a fundamental characteristic of rat spermatogenic cells and Sertoli cells. Proc. Natl. Acad. Sci. USA *105*, 8315–8320. https://doi.org/10.1073/pnas.0709854105.

44. Klaus, E.S., Gonzalez, N.H., Bergmann, M., Bartkuhn, M., Weidner, W., Kliesch, S., and Rathke, C. (2016). Murine and Human Spermatids Are

Characterized by Numerous, Newly Synthesized and Differentially Expressed Transcription Factors and Bromodomain-Containing Proteins. Biol. Reprod. *95*, 4. https://doi.org/10.1095/biolreprod.115.137620.

45. Wolf, F.A., Angerer, P., and Theis, F.J. (2018). SCANPY: large-scale single-cell gene expression data analysis. Genome Biol. *19*, 15. https://doi.org/10.1186/s13059-017-1382-0.

46. Palla, G., Spitzer, H., Klein, M., Fischer, D., Schaar, A.C., Kuemmerle, L.B., Rybakov, S., Ibarra, I.L., Holmberg, O., Virshup, I., et al. (2022). Squidpy: a scalable framework for spatial omics analysis. Nat. Methods *19*, 171–178. https://doi.org/10.1038/s41592-021-01358-2.

47. Yu, G., Wang, L.G., Han, Y., and He, Q.Y. (2012). clusterProfiler: an R package for comparing biological themes among gene clusters. OMICS *16*, 284–287. https://doi.org/10.1089/omi.2011.0118.

## STAR★METHODS

### KEY RESOURCES TABLE

| REAGENT or RESOURCE | SOURCE | IDENTIFIER |
|---|---|---|
| Antibodies | | |
| Mouse Anti-CYP11A1 | Proteintech | Cat# 67264-1-Ig; RRID: AB_2882535 |
| Rabbit anti-PTN | Proteintech | Cat# 27117-1-AP; RRID: AB_2880763 |
| Goat anti-PTN | R&D Systems | Cat# AF252SP; RRID: AB_2300563 |
| Mouse anti-Syndecan-4 (5G9) Alexa Fluor® 546 | Santa Cruz Biotechnology | Cat# sc-12766 AF546; RRID: AB_628314 |
| Rabbit anti-Ephrin A1 | Abcam | Cat# ab124911; RRID: AB_10974078 |
| Mouse anti-VWF | Proteintech | Cat#: 66682-1-Ig; RRID: AB_2882036 |
| Mouse anti-GFRa1 Alexa Fluor® 647 | Santa Cruz Biotechnology | Cat# sc-271546 AF647; RRID: AB_10649373 |
| Alexa Fluor 488 Secondary Antibody | Thermofisher Scientific | Cat# A-11008; RRID: AB_143165 |
| Alexa Fluor 594 Secondary Antibody | Thermofisher Scientific | Cat# A-11012; RRID: AB_141359 |
| Alexa Fluor 647 Secondary Antibody | Thermofisher Scientific | Cat# A-21447; RRID: AB_141844 |
| Goat anti-GFRa1 | R&D Systems | Cat# AF714; RRID: AB_355541 |
| PE rat anti-human CD49f/ITGA6 | BD Biosciences | Cat# 555736; RRID: AB_396079 |
| APC mouse anti-human CD117/KIT | BD Biosciences | Cat# 550412; RRID: AB_398461 |
| Biological samples | | |
| Human Testis Tissue Samples | Kyle Orwig Lab | N/A |
| Mouse Testis Tissue Samples | Haiqi Chen Lab | N/A |
| Chemicals, peptides, and recombinant proteins | | |
| Human Recombinant GDNF | R&D Systems | Cat# 212-GD-050 |
| Rat Recombinant GFRa1 | R&D Systems | Cat# 560-GR-100 |
| Recombinant FGF2 | Invitrogen | Cat# 13256-029 |
| Recombinant PTN | R&D Systems | Cat# 252-PL |
| DAPI | Sigma-Aldritch | Cat# D9542 |
| ProLong™ Gold Antifade Mountant | Sigma-Aldritch | Cat# P36934 |
| Hank's Balanced Salt Solution (HBSS) | Thermo Fisher | Cat # 24020-117 |
| Collagenase IV | Worthington Biochemical | Cat# LS004188 |
| Trypsin-EDTA | Thermo Fisher | Cat# 25200114 |
| DNase I | Worthington Biochemical | Cat# LS002147 |
| DPBS | Thermo Fisher | Cat# 14200-075 |
| FBS | Thermo Fisher | Cat# 10082-147 |
| Anti-PE Microbeads | Milteny Biotec | Cat# 130-048-801 |
| StemPro-34TM SFM Media | Thermo Fisher | Cat# 10639011 |
| bFGF | Thermo Fisher | Cat# 13256-029 |
| Human Ephrin-A1 (EFNA1) | R&D Systems | Cat# 6417-A1 |
| 0.5% Trypsin EDTA | Gibco | Cat# 25300120 |
| Ghost Dye™ Red 780 | Tonbo Biosciences | Cat# 13-0865-T100 |
| 1:1 Perm/Wash Buffer | BD Biosciences | Cat# 554723 |
| UltraComp eBeads™ | ThermoFisher | Cat# 01-2222-42 |
| Critical commercial assays | | |
| Illumina NovaSeq 100 Cycle Reagent kit | Illumina | Cat# 20028319 |
| Nextera XT DNA Library Preparation Kit (96 samples) | Illumina | Cat# FC-131-1096 |
| Slide-seq Arrays | Fei Chen Lab | N/A |
| Dead Cell Removal Kit | Milteny Biotec | Cat# 130-090-101 |

(*Continued on next page*)

*Continued*

| REAGENT or RESOURCE | SOURCE | IDENTIFIER |
|---|---|---|
| Deposited data | | |
| Raw Slide-seq data | GEO | BioProject ID: PRJNA668433 |
| Additional raw Slide-seq data | UTSW Cloud Drive | https://cloud.biohpc.swmed.edu/index.php/s/oCBrZWj6JGjC8E9 |
| Processed data | Github | https://github.com/thechenlab/Testis_Slide-seq |
| Additional processed data | UTSW Cloud Drive | https://cloud.biohpc.swmed.edu/index.php/s/nCM8Px3zFmTpZrk |
| Processed LR interaction data | Single Cell Portal | Portal ID: SCP2166 |
| Experimental models: Organisms/strains | | |
| Mouse: 129/SvEv x B6 F1 Hybrids | Makoto Nagano Lab | N/A |
| Mouse: C57BL/6J | The Jackson Laboratory | Strain #:000664 |
| Oligonucleotides | | |
| Template Switch Oligo (AAGCAGTGGTATCA ACGCAGAGTGAATrG+GrG) | This paper | N/A |
| SMART_PCR_Primer (AAGCAGTGGTATCAACGCAGAGT) | This paper | N/A |
| Truseq_PCR_Handle (CTACACGACGCTCTTCCGATCT) | This paper | N/A |
| Truseq P5 (AATGATACGGCGACCACCGAGATCTA CACTCTTTCCCTACACGACGC TCTTCCGATCT) | This paper | N/A |
| dN-SMRT oligo (AAGCAGTGGTATCAACGCAGAG TGANNNGGNNNB) | This paper | N/A |
| HCR probes | Molecular Instruments | N/A |
| Software and algorithms | | |
| Testis Slide-seq data analysis | In house | https://github.com/HaiqiChenLab/Slideseq_SSC_Niche |
| Slide-seq tools | In house | https://github.com/MacoskoLab/slideseq-tools |
| RCTD | Cable et al.[17] | https://github.com/dmcable/spacexr |
| NICHES | Raredon et al.[18] | https://github.com/msraredon/NICHES |
| COMMOT | Cang et al.[26] | https://github.com/zcang/COMMOT |

## RESOURCE AVAILABILITY

### Lead contact

Further information and requests for resources and reagents should be directed to and will be fulfilled by the lead contact, Haiqi Chen (haiqi.chen@utsouthwestern.edu).

### Materials availability

This study did not generate new unique reagents.

### Data and code availability

- The raw sequencing data supporting the findings of this study are available in the NCBI BioProject database (BioProject ID: PRJNA668433) and at https://cloud.biohpc.swmed.edu/index.php/s/oCBrZWj6JGjC8E9. The newly generated, processed data including the gene expression matrix and the bead location matrix can be found at https://cloud.biohpc.swmed.edu/index.php/s/nCM8Px3zFmTpZrk. Previously generated, processed data including the gene expression matrices and bead location matrices are available at https://github.com/thechenlab/Testis_Slide-seq. A data visualization portal using the framework of Single Cell Portal can be access through the following link https://singlecell.broadinstitute.org/single_cell/study/SCP2166/testis-slide-seq.
- Custom code is available at https://github.com/HaiqiChenLab/Slideseq_SSC_Niche.
- Any additional information required to reanalyze the data reported in this paper is available from the lead contact upon request.

## EXPERIMENTAL MODEL AND STUDY PARTICIPANT DETAILS

### Animals

Mouse testis tissue collection for Slide-seq and IF were carried out with prior approval of the UT Southwestern Medical Center on Use and Care of Animals, in accordance with the guidelines established by the National Research Council Guide for the Care and Use of Laboratory Animals. Adult (7–18 weeks old) C57BL/6J (B6) male mice were housed in the UT Southwestern Medical Center animal facility, in an environment controlled for light (12 h on/off) and temperature (21–23°C) with *ad libitum* access to water and food.

All procedures for handling and care of mice for spermatogonial culture and transplantation experiments were approved by the Animal Care and Use Committee of the Research Institute of the McGill University. 6- to 9-day old F1 pups of B6 and B6.129S7-Gtrosa26Sor, the latter of which carries the bacterial β-galactosidase, served as donor miceand were used to isolate spermatogonia. The recipient mice for spermatogonial transplantation were 129/SvEv x B6 F1 hybrids. All mice were housed in an environment controlled for light (12 h on/off) and temperature (21–23°C) with *ad libitum* access to water and food.

### Human samples

Adult human testicular samples were from four healthy men (donor #1: 21 years old; donor #2: 24 years old; donor #3: 32 years old; donor #4: 48 years old; unknown races); Samples were obtained through the University of Pittsburgh Health Sciences Tissue Bank and Center for Organ Recovery (CORID No. 686). All samples were de-identified.

### Primary cell cultures

Mouse SSCs were isolated from 6- to 9-day old male F1 pups of B6 and B6.129S7-Gtrosa26Sor parents and were cultured *in vitro*. Human SSCs were isolated from human testicular samples described above and were cultured *in vitro*. See below for culture details.

## METHOD DETAILS

### Slide-seq workflow

Slide-seq arrays were gifts from Fei Chen at the Broad Institute of MIT and Harvard. Fresh frozen testis tissue sections at 10 μm thickness were obtained using a cryostat (Leica CM3050S), and then moved onto the Slide-seq arrays. The arrays were then placed into a 1.5 mL microcentrifuge tube. The sample library was then prepared based on the protocol detailed before.[15,34] Library quantification was performed using the Bioanalyzer. The library concentration was normalized to 4 nM for sequencing. Samples were sequenced on the Illumina NovaSeq S2 flow cell 100 cycle kit with the read structure 42 bases Read 1, 8 bases i7 index read, 50 bases Read 2. Each bead array received approximately 150–200 million reads, corresponding to ~2,000–2,500 reads per bead.

### Immunofluorescence

Slides with tissue sections were fixed in 4% PFA (in PBS) and washed three times in PBS for 5 min each, blocked 30 min in 4% BSA (in PBST), incubated with primary antibodies overnight at 4°C, washed three times in PBS for 5 min each, and then incubated with secondary antibodies at for 1 h at room temperature. Slides were then washed twice in PBS for 5 min each and then for 10 min with a PBS containing DAPI (D9542, Sigma-Aldrich). Lastly, slides were mounted using ProLong Gold Antifade Mountant (P36934, Thermo Fisher Scientific) and sealed. Antibodies used for IF: mouse Anti-CYP11A1 antibody (1:200, 67264-1-Ig, Proteintech), rabbit anti-PTN antibody (1:100, 27117-1-AP, Proteintech), goat anti-PTN antibody (1:100, AF252SP, R&D Systems), mouse anti-Syndecan-4 (5G9) Alexa Fluor 546 antibody (1:100, sc-12766 AF546, Santa Cruz Biotechnology), rabbit anti-Ephrin A1 antibody (1:100, ab124911, abcam), mouse Anti-VWF antibody (1:100, 66682-1-Ig, Proteintech), mouse anti-GFRa1 Alexa Fluor 647 antibody (1:100, sc-271546 AF647, Santa Cruz Biotechnology) and Alexa Fluor 488-, 594-, and 647-conjugated secondary antibodies (Thermo Fisher Scientific). Imaging was performed using an inverted Nikon CSU-W1 Yokogawa spinning disk confocal microscope with a Nikon CFI APO LWD 40X/1.15 water immersion objective and an Orca-Fusion GEN-III sCMOS camera.

### smFISH

smFISH was performed using the hybridization chain reaction (HCR) technique as described before.[15] Reagents and gene probes were purchased from Molecular Instruments. Briefly, frozen testes were sectioned into (3-Aminopropyl) triethoxysilane-treated glass bottom 24-well plates. Sections were cross-linked with 10% Formalin for 15 min, washed with 1X PBS for three times, and permeabilized in 70% ethanol for 2 h - overnight at −20°C. Sections were then rehydrated with 2X SSC for three times and equilibrated in HCR hybridization buffer for 10 min at 37°C. Gene probes were added to the sections at a final concentration of 2 nM in HCR hybridization buffer and hybridized overnight in a humidified chamber at 37°C. After hybridization, samples were washed four times in HCR wash buffer for 15 min at 37°C and then three times for 5 min at room temperature in 5X SSCT. The probe sets were amplified with HCR hairpins for 12–16 h at room temperature in HCR amplification buffer. Prior to use, the hairpins were 'snap cooled' by heating at 95°C for 90 s and letting cool to room temperature for 30 min in the dark. After amplification, the samples were washed in 5X SSCT and stained with 20 ng/mL DAPI before imaging. Microscopy was performed using an inverted Nikon CSU-W1 Yokogawa spinning disk confocal microscope with 488 nm, 640nm, 561nm, and 405 nm lasers, a Nikon CFI APO LWD 40X/1.15 water immersion objective, and an ORCA-FUSION GEN-III sCMOS camera. NIS-Elements AR software (v4.30.01, Nikon) was used for image capture.

### Culture of mouse spermatogonia for the transplantation assay

The culture was established as described previously[35] using Thy1-positive spermatogonia from 6- to 9-day old pups (designated B6ROSA26). These donor mice were the F1 progeny of B6 and B6.129S7-Gtrosa26Sor, the latter of which carries the bacterial β-galactosidase in virtually all cell types. Cells were placed initially in the wells of 24-well plates at 0.2 x $10^6$ cells/well. They were cultured on an STO feeder layer with culture medium supplemented with recombinant human GDNF (212-GD-050, R&D Systems) at 20 ng/mL, recombinant rat GFRa1 (560-GR-100, R&D Systems) at 75 ng/mL, FGF2 (13256-029, Invitrogen) at 1 ng/mL, and 0, 5, or 50 ng/mL of recombinant PTN (252-PL, R&D Systems). The dosages of PTN were selected based on a previous study.[36] Culture medium was replaced every 3 to 4 days, and spermatogonia were subcultured every week at a 1:2 split rate four times; thus, the total culture period was 5 weeks up to transplantation.

### Transplantation assay

The recipient mice for spermatogonial transplantation were 129/SvEv x B6 F1 hybrids. These mice were treated with an i.p.-injection of busulfan at 50 mg/kg body weight at 4 weeks of age and served as recipients of transplantation 7 to 8 weeks later.[37] Cultured mouse spermatogonia were harvested by trypsinization and a single-cell suspension was made at ~$10^6$ cells/mL. These cells were injected into the seminiferous tubules of recipients through efferent ducts using micropipettes.[37,38] Two months after transplantation, recipient testes were recovered and stained with X-gal to count the number of colonies derived from donor spermatogonia. The colony number indicates the number of SSCs successfully engrafted after transplantation. The count data was normalized as "per culture well" for fair comparisons across the treatment groups.[39]

### Isolation of human spermatogonia and culture

To investigate the effects of Ephrin-A1 on human spermatogonial cells *in vitro*, culture of spermatogonial cells was performed as previously described.[40] Briefly, cryopreserved human testicular tissues from four adult donors (21, 24, 32, and 48 years old, respectively) were thawed quickly in a 37°C water bath and washed in Hank's Balanced Salt Solution (HBSS) (24020-117, Gibco). Tissues were then digested sequentially with 2 mg/ml Collagenase IV (LS004188, Worthington Biochemical), 0.25% Trypsin-EDTA (25200114, Thermo Fisher), and 3.5 mg/ml DNase I (LS002147, Worthington Biochemical) in HBSS at 37°C. The cell suspension obtained was filtered through a 40 μm cell strainer (08-771-1, Thermo Fisher), and dead cells were removed through magnetic activated cell sorting (MACS) using the Dead Cell Removal Kit (130-090-101, Milteny Biotec). MACS-sorted live cells were stained with PE rat anti-human CD49f/ITGA6 (10 μL/$10^6$ cells, 555736, BD Biosciences) in 1X DPBS (14200-075, Gibco) supplemented with 1% FBS (10082-147, Gibco), then incubated in DPBS containing anti-PE MicroBeads (2 μL/$10^6$ cells, 130-048-801, Milteny Biotec). The ITGA6+ fraction was collected in StemPro-34TM SFM media (10639011, Thermo Fisher) supplemented with GDNF (450-010, Peprotech) at 20 ng/mL and bFGF (13256-029, Thermo Fisher) at 1 ng/mL. Cells were then seeded on human collagen I-coated 6-well plates (1 μg/$cm^2$; 08-774-550, Corning) to remove adherent somatic cells. After 24 h at 37°C, floating cells were removed and re-plated on fresh collagen I-coated wells for additional 24 h. In the following day, the remaining floating cells were collected for cell culture.

To culture human spermatogonia, human testis-derived extracellular matrix (htECM) was neutralized to pH 7.6 using 0.1 N NaOH and diluted in 1X DPBS for coating 24-well plates at a final concentration of 300 μg/mL for 2 h at room temperature. At the time of seeding ITGA6$^+$ MACS-sorted cells, wells containing residual htECM were washed with HBSS and the cells were plated at a concentration of 2.5-5x$10^4$ cells/$cm^2$ in three different GDNF/bFGF supplemented StemPro-34TM SFM media with: 0 ng/mL, 3 ng/mL, and 6 ng/mL of recombinant human Ephrin-A1 (EFNA1, 6417-A1, R&D Systems). The concentration of EFNA1 used in this study was determined according to manufacturer's instructions that approximately 0.6–3 ng/mL produces 50% of the optimal binding response measured by ELISA. Fresh medium was added into culture wells every 3–4 days and cells were collected at day 0, and day 7 after trypsinization (0.05% Trypsin EDTA, 25300120, Gibco).

### Multiparameter FACS

To evaluate the presence of undifferentiated (GFRa1$^+$) and differentiated (Kit$^+$) spermatogonia through FACS, we followed the method previously reported by Murdock et al.[40] In short, cultured human spermatogonia were washed with azide-free and serum-free 1X DPBS (DPBS-S, 14200-075, Gibco) and incubated with the viability dye Ghost Dye Red 780 (13-0865-T100, Tonbo Biosciences) according to the manufacturer's instructions. Cells were washed and incubated in 1X DPBS (DPBS-S, 14200-075, Gibco) containing 1% FBS (10082-147, Gibco), goat anti-GFRa1 antibody (5μL/$10^6$ cells; AF714, R&D Systems) and APC mouse anti-human CD117/KIT antibody (5μL/$10^6$ cells, 550412, BD Biosciences) for 25 min on ice. Cells were then washed and incubated with fluorescent secondary antibodies. After washing, cells were fixed in 4% PFA for 15 min at room temperature and washed in 1:1 Perm/Wash buffer (554723, BD Biosciences). After being washed and filtered through 40 μm strainers (08-771-1, Thermo Fisher), samples were analyzed using the BD FACSAria II flow cytometer. Unstained cells were used as the negative control. Compensation controls were prepared using UltraComp eBeadsTM (01-2222-42, ThermoFisher) incubated with isotype antibody controls for each fluorophore according to manufacturer instructions.

## Computational methods for slide-seq data

### *Preprocessing of slide-seq data*

The Slide-seq tools (https://github.com/MacoskoLab/slideseq-tools) were used for processing raw sequencing data. In brief, low-quality reads were filtered and trimmed. STAR[41] was used to align reads to genome sequence. The Slide-seq tools extracted cellular barcode (i.e., bead spatial barcode) and molecular barcode (UMI) from aligned reads. For each of those cellular barcodes, hamming distances were calculated between it and all the cellular barcodes from *in situ* sequencing. The list of uniquely matched bead barcodes was outputted. The final output from the Slide-seq tools were a digital gene expression matrix (bead barcodes X genes) and barcode location matrix (bead barcodes X spatial coordinates). For each Slide-seq bead, the total number of UMIs were calculated and beads with less than 20 UMIs were filtered out. A trimming step was also applied to exclude beads located outside the main area of the bead array.

## Cell type assignment

RCTD was used to accurately assign cell types and SPG subtypes to Slide-seq beads.[17] The method consisted of two main steps: first, scRNA-seq data previously annotated with cell type identities was used to calculate the mean gene expression profile of each cell type and SPG subtype. Next, RCTD created a spatial map of cell types/subtypes by fitting the spatial transcriptomics of each Slide-seq bead as a linear combination of individual cell types/subtypes. Cell type/subtype weights and a bead class (one of the following: singlet, doublet, and reject) were assigned to each bead. Beads with the bead class as 'reject' were removed from downstream analysis. The cell types/subtypes of the remaining beads were assigned based on the identity of the cell type/subtype with the largest weight. To perform RCTD on the mouse slide-seq data, we used scRNA-seq data from a study by Green et al.[16] For the human Slide-seq data, we used data from Guo et al. as a ref. 24.

## Assignment of stages of the cycle of the seminiferous epithelium

To assign stage information to each Slide-seq bead, first, a pseudotime value was assigned to each bead using a previously established method.[15] Next, the Slide-seq pseudotime data was converted into a grayscale image followed by Gaussian smoothing, thresholding, watershed segmentation, and *K*-nearest neighbor (KNN) analysis[15] (Figure S1G). The result was the assignment of each Slide-seq bead to a seminiferous tubule. Segmented seminiferous tubules with a total number of beads less than 20 and more than 700 were first filtered out. This was because tubules with less than 20 beads usually only represented a small portion of a tubule and tubules containing more than 700 beads represented two tubules which were not properly separated by the algorithm. The raw unique molecular identifier (UMI) count data of the Slide-seq beads was then normalized and variance-stabilized using the function SCTransform from Seurat V3.[42] The normalized gene expression values of the Slide-seq beads within the same tubule were aggregated. Uniform manifold approximation and projection (UMAP) for dimension reduction of the aggregated gene expression data were performed using the top 3000 highly variable genes under the assumption that seminiferous tubules at similar stages should share similar transcriptional profiles. Finally, genes whose expressions are known to be stage-specific[43,44] were used to assign stages to each cluster (Figure S1H). These genes include *H1fnt*, *H3f3b*, *Tnp1*, *Prm1*, *Prm2*, *Serpina3a*, *Smcp*, *Ssxb1*, *Taf2*, *Pcaf*, *H2A*, *Ezh2*, *Brd8*, *Taf5*, *Trim24*, and *Brd2*.

## Generation of a spatially resolved LR interaction map

NICHES[18] was adopted to survey the LR interaction landscape using the Slide-seq data. For each Slide-seq bead, a mutual KNN graph was computed based on the spatial coordinates of the beads. K = 4 neighbors were used for building the nearest neighbor graphs. K = 10 was also tested and yielded similar results (data not shown). The expression level of each LR pair was calculated by multiplying ligand expression on the sending cell with receptor expression on the receiving cell. The spatial expression of each LR pair was then visualized using Scanpy.[45] The bead-LR pair expression matrix was used to create a Seurat object, with the cell type and stage information of each Slide-seq bead as meta data. The normalized and scaled LR-pair expression data was subject to low-dimensional embedding using UMAP and was then used to identify the stage-specific expression of LR pairs using the FindAllMarkers function from Seurat V3. To dissect the interactions between each cellular component of the niche and the SSCs, the expression of LR pairs coming from each niche component and landing on the SPG1 cell population was computed by summing the expression of the LR pairs from beads belonging to the queried cell types. Cell type-specific expressions of LR pairs were then identified using the FindAllMarkers function.

## Calculation of signaling activities and signaling directions

COMMOT[26] was adopted to infer signaling activities and spatial signaling directions. To achieve this, ligand and receptor expression were viewed as two distributions to be coupled with a cost based on spatial distance to form an Optimal Transport problem. A collective optimal transport approach was developed to reconstruct signaling activities based on LR expressions. The spatial signaling direction was obtained by interpolating a cell-by-cell cell-cell communication matrix to a vector field in the intact tissue space to describe from or to what direction was the signal received or sent.

### Neighborhood enrichment analysis

To dissect the spatial relationship between SPG subtypes, an enrichment score was calculated. First, a connectivity matrix from spatial coordinates of the Slide-seq beads assigned as the SPG subtypes was computed. Next, the spatial association between each SPG subtype pair in the connectivity graph was estimated by counting the sum of nodes that belong to the SPG subtype pair and were proximal to each other. The number of observed nodes was compared against 100 permutations and a *Z* score was computed. This analysis was implemented in the gr.nhood_enrichment function from Squidpy.[46]

### Calculation of the spatial autocorrelation score

The spatial autocorrelation score was adopted from the Moran's I global spatial auto-correlation statistics which evaluates whether features (in our case, the expression of an LR pair) show a pattern that is clustered, dispersed, or random in the tissue. We found that only positive spatial autocorrelation scores were generated for the LR pairs. This implies that the expression of LR pairs tend to cluster spatially (i.e., Slide-seq beads with high expression values cluster near each other, and beads with low values cluster near other beads with low values). To enable the comparison between the WT and *ob/ob* samples, we assumed that the overall size and structure of the profiled tissue areas of the two groups were largely similar. Only the *Z* score from the Moran's I statistics with a multiple hypothesis-corrected p value less than 0.05 was used for comparison.

### Validation of the spatial autocorrelation score analysis

To test if the spatial autocorrelation score captures real changes in the spatial expression patterns of LR pairs in the *ob/ob* vs. WT testes, a generalized linear spatial model-based statistical method called SPARK[32] was applied to individual seminiferous tubules. For each queried LR pair, whether its spatial expression pattern is statistically non-random in the *ob/ob* vs. WT tubules was determined by SPARK using default settings. We looked for LR pairs whose expression show non-random spatial distribution in the WT tubules but not in the *ob/ob* tubules.

### GO analysis

GO analysis was performed using the clusterProfiler package.[47] Cellular components from the org.Mm.eg.db genome wide annotation for the mouse was used for the ontology database.

## QUANTIFICATION AND STATISTICAL ANALYSIS

All experiments were reproduced at least twice unless stated otherwise. Transplantation data were obtained from two series of spermatogonial cultures, involving at least 12 testes for each group. Significance was determined using one-way ANOVA followed by the Fisher's Least-Significant-Difference Test, and $p < 0.05$ was determined to be significant. FACS data of human spermatogonia were obtained from 4 patient samples. To enable comparison between groups, log2 transformed data on the percentage of each SPG stage were used. Significance was determined using one-way ANOVA followed by Tukey's Test, and $p < 0.05$ was determined to be significant. Comparison of the spatial autocorrelation scores between the WT and *ob/ob* tubules were performed using Wilcoxon rank-sum test.